Since January 2020 Elsevier has created a COVID-19 resource centre with free information in English and Mandarin on the novel coronavirus COVID-19. The COVID-19 resource centre is hosted on Elsevier Connect, the company's public news and information website.

BASIC SCIENCE

Nanomedicine: Nanotechnology, Biology, and Medicine
47 (2023) 102624

Original Article

nanomedjournal.com

Simultaneously ultrasensitive and quantitative detection of influenza A virus, SARS-CoV-2, and respiratory syncytial virus via multichannel magnetic SERS-based lateral flow immunoassay

Zhenzhen Liu, MSc, Chongwen Wang, PhD, Shuai Zheng, PhD, Xingsheng Yang, PhD, Han Han, MSc, Yuwei Dai, MSc, Rui Xiao, PhD*

[a]*Beijing Institute of Microbiology and Epidemiology, Beijing, PR China*
[b]*Beijing Key Laboratory of New Molecular Diagnosis Technologies for Infectious Diseases, Beijing 100850, PR China*

Revised 30 July 2022

Abstract

Respiratory viruses usually induced similar clinical symptoms at early infection. Herein, we presented a multichannel surface-enhanced Raman scattering-based lateral flow immunoassay (SERS-based LFA) using high-performance magnetic SERS tags for the simultaneous ultrasensitive detection of respiratory viruses, namely influenza A virus (H1N1), severe acute respiratory syndrome coronavirus 2 (SARS-CoV-2) and respiratory syncytial virus (RSV) in biological samples. As-prepared magnetic SERS tags can directly enrich and capture target viruses without pretreatment of samples, avoiding the interference of impurities in the samples as well as improving the sensitivity. With the capture-detection method, the detection limits of the proposed assay reached 85 copies mL^{-1}, 8 pg mL^{-1}, and 8 pg mL^{-1} for H1N1, SARS-CoV-2 and RSV, respectively. Moreover, the detection properties of the proposed method for target viruses in throat swab samples were verified, suggesting its remarkable potential for the early and rapid differential diagnosis of respiratory viruses.

Keywords: SERS-based lateral flow immunoassay; Magnetic tags; Fe_3O_4@Au; Respiratory viruses; Simultaneous detection

Respiratory viruses with high infectivity, short latency, and acute incidence, primarily spread by breathing and humors, resulting in approximately four million deaths of infections every year.[1] The worldwide outbreak of the coronavirus disease-2019 (COVID-19) has attracted people's comprehensive attention to the pathogenetic respiratory viruses again. And the severe acute respiratory syndrome coronavirus 2 (SARS-CoV-2) was known to the culprit of COVID-19. Due to its high infectivity rate, SARS-CoV-2 has caused over 6 million deaths among 500 million confirmed cases globally to date.[2] In addition, several studies have reported co-infections of SARS-CoV-2 and other respiratory viruses such as influenza A, influenza B (Flu B) and respiratory syncytial virus (RSV).[3,4] Patients infected by these respiratory viruses mostly experienced from non-symptomatic to mild symptoms, severe respiratory symptoms, and even death[5]. Considering the similar symptoms and transmission, the early and accurate diagnosis of pathogenic viruses is the key step for early treatment and urgent prevention.[6]

Current detecting methods for respiratory viruses, such as the isolation and culture[7], polymerase chain reaction (PCR)[8,9], and enzyme-linked immunosorbent assay (ELISA)[10], equipped with high sensitivity. But they required rigorous conditions, time-consuming steps, sophisticated instruments, and skilled researchers. In addition, as the detectable levels of anti-virus (e.g., SARS-CoV-2) antibodies usually took 10 or more days after symptom onset, the direct detection of antigen is vital for early diagnose and community screening.[11] Lateral flow immunoassay (LFA) such as conventional colloidal gold-LFA is considered as the most potential point of care testing (POCT) method with simple operation, low cost, and short reaction time.[12,13] Nevertheless, the suboptimal sensitivity and non-quantitative analysis limit its application. Therefore, a rapid, highly sensitive and quantitative method for the detection of respiratory viruses at POCT is urgently needed.

Recently, surface-enhanced Raman scattering (SERS) has increasingly attracted researchers' attention with high sensitivity,

* Corresponding author.
E-mail address: ruixiao203@sina.com (R. Xiao).

https://doi.org/10.1016/j.nano.2022.102624
1549-9634/

Please cite this article as: Liu Z, et al, Simultaneously ultrasensitive and quantitative detection of influenza A virus, SARS-CoV-2, and respiratory syncytial virus via multichannel magnetic SERS-based lateral flow immunoassay. *Nanomedicine: NBM* 2023;47:102624, https://doi.org/10.1016/j.nano.2022.102624

narrow bandwidth, and multichannel detection.[14,15] Moreover, SERS-based LFA remarkably improved the ability of sensitive and quantitative detection, and widely used in the analysis of nucleic acids[16], proteins[17,18], bacteria[19], and viruses[20,21]. Notably, the detecting capability of SERS-based LFA depended on the SERS tags to a great extent. Several reports have suggested that the Raman signal of molecules is usually higher while at the tips of the plasmon and amplified remarkably while conjugated with noble metals (e.g., silver, gold, and copper).[22,23] Researchers have fabricated many high-performance SERS substrates such as gold nanorods (Au NRs), hollow gold nanospheres, Au@Ag NPs, $MnFe_2O_4$@Au NPs, and so on.[24–26] Maneeprakorn et al. reported a gold nanostars as SERS tags for influenza A nucleoprotein detection with a low detection limit of 6.7 ng mL^{-1}.[27] Wang et al. proposed a SERS-based LFA via Fe_3O_4@Ag tags for simultaneous detection of influenza A and human adenovirus (HAdV) with the sensitivity of 2000 times lower than conventional colloidal gold-LFA.[21] Liu et al. prepared SiO_2@Ag NPs as SERS tags for the detection of anti-SARS-CoV-2 IgM/IgG.[28] However, though the SERS performance greatly enhanced with Ag shell coated on Fe_3O_4 or SiO_2, the stability and oxidation resistance of Ag are weak, and the corresponding SERS signals will decrease with the long-term exposure to the air[29,30].

In addition, due to the excellent enrichment capability, immunomagnetic nanomaterials (e.g., Fe_3O_4 NPs) were introduced to target detection in complex samples such as serum and food samples.[31] Furthermore, the magnetic tags can directly capture and enrich target analytes from the complex samples by external magnet without pretreatment. And the enriched compound was resuspended in running buffer for the following detection, eliminating the interference of the impurities in the sample. Such character of magnetic tags exactly solves the problem of respiratory viruses' detection in nasopharyngeal and throat swabs. In detail, the swabs with complex ingredients would influence the detecting results by reducing the speed of chromatography and resulting in nonspecific adsorption.[32]

In this study, we propose a multichannel SERS-based LFA strips based on Fe_3O_4@Au MNPs for the simultaneous and ultrasensitive detection of three respiratory viruses (H1N1/SARS-CoV-2/RSV). Notably, Au coated on Fe_3O_4 NPs showed excellent chemical and optical stability, and its oxidation resistance is stronger than silver.[33] In addition, dual-layer of Raman report molecule, namely, 5,5′-dithiobis-(2-nitrobenzoic acid) (DTNB) were modified on Fe_3O_4@Au MNPs to prepare magnetic SERS tags, providing high SERS signals and abundant binding sites for antibodies. Based on antigen-antibody reaction, magnetic SERS tags could form a sandwich-like structure on the test (T) lines together with target viruses and antibodies. The quantitative detection of H1N1/SARS-CoV-2/RSV virions is realized by measuring the SERS signals on three T lines via our proposed SERS-based LFA strips. By optimizing, the sensitivity values of Fe_3O_4@Au-based SERS strips for the detection of H1N1, SARS-CoV-2 and RSV achieve 85 copies mL^{-1}, 8 pg mL^{-1}, and 8 pg mL^{-1}, respectively, which are 100 times more sensitive than those of colloidal Au NP-based LFA strips. Furthermore, inactive SARS-CoV-2 and RSV virions have been tested by our proposed strips to verify the clinical utility. And the performances of our method, such as accuracy, specificity, and stability, are also demonstrated. All results exhibit the remarkable potential of our magnetic SERS-based LFA strips in the accurate diagnosis of respiratory diseases under POCT field.

Methods

Chemicals and materials

Ferric chloride ($FeCl_3{\cdot}6H_2O$), chloroauric acid tetrahydrate ($HAuCl_4{\cdot}4H_2O$) and hydroxylamine hydrochloride ($NH_2OH{\cdot}HCl$) were purchased from Shanghai Chemical Reagent Co. (China). PEI, polyvinylpyrrolidone (PVP), DTNB, 2-(N-morpholino) ethanesulfonic (MES), N-hydroxysuccinimide (NHS), N-(3-dimethylaminopropyl)-N′-ethylcarbodiimide hydrochloride (EDC), and bovine serum albumin (BSA) were obtained from Sigma-Aldrich (USA). Deionized water acquired by the Millipore Milli-Q system was used to prepare all aqueous solutions. The components of chromatography strip except nitrocellulose membrane, which was purchased from Sartorius (Spain), were purchased from Jieyi Biotechnology Co., Ltd. (Shanghai, China).

Goat anti-mouse IgG was purchased from Sangon Biotech Co., Ltd. (Shanghai, China). Mouse monoclonal anti-H1N1 antibodies (catalog no. FLUA-REAB-G1–006 and FLUA-REAB-G1–007) and mouse monoclonal anti-RSV (catalog no. 2 and 9) were provided by Fapon Biotech Inc. (China). SARS-CoV-2 SP (catalog no. V08B2), mouse monoclonal anti-SARS-CoV-2 SP antibodies (catalog no. D002 and D004), commercial ELISA kits for Influenza H1N1 (catalog no. 11055), SARS-CoV-2 spike protein (catalog no. 40591), and RSV (catalog no. 11049) were obtained from Sino Biological Inc. (China). The RSV protein (30–1966) was purchased from Fitzgerald (USA).

Influenza A (H1N1 2009/A) were cultured in chick embryos and quantitated by PCR in our laboratory. In addition, Flu B and HAdV both obtained from our laboratory. Inactivated SARS-CoV-2 (~10^8 copies mL^{-1}) were supplied by Prof. Qin's laboratory in Beijing Institute of Microbiology and Epidemiology [5] and RSV (~10^6 $TCID_{50}$ mL^{-1}) virions were purchased from Nanjing Baikang Bio, Ltd. (China). The middle east respiratory syndrome coronavirus (MERS) protein (catalog no. V08B1) was purchased from Sino Biological Inc. (Beijing, China).

Synthesis of dual-layer DTNB-modified monodispersed Fe_3O_4@Au MNPs

The dual-layer DTNB-modified monodispersed Fe_3O_4@Au MNPs were prepared using the PEI-mediated seed growth method shown in Scheme. 1A, as reported in our previous studies.[34,35] Briefly, PEI was first absorbed on to the surface of Fe_3O_4 MNPs to shape up Fe_3O_4/PEI. And then the small Au NPs (~3 nm) were adhered to the Fe_3O_4/PEI by electrostatic interactions to shape up Fe_3O_4-Au seeds with ultrasonic. Next, the freshly prepared DTNB-ethanol solution was added to the above seeds under sonicating to form the first layer of DTNB on Fe_3O_4-Au seeds. With the functions of PVP and $NH_2OH{\cdot}HCl$, the Au shell originated from $HAuCl_4$ solution was grown on the seeds to form Fe_3O_4@Au core–shell MNPs under sonicating. The second layer of DTNB was modified onto the surface of the shell under the same condition. The detailed process was illustrated in Supporting Information.

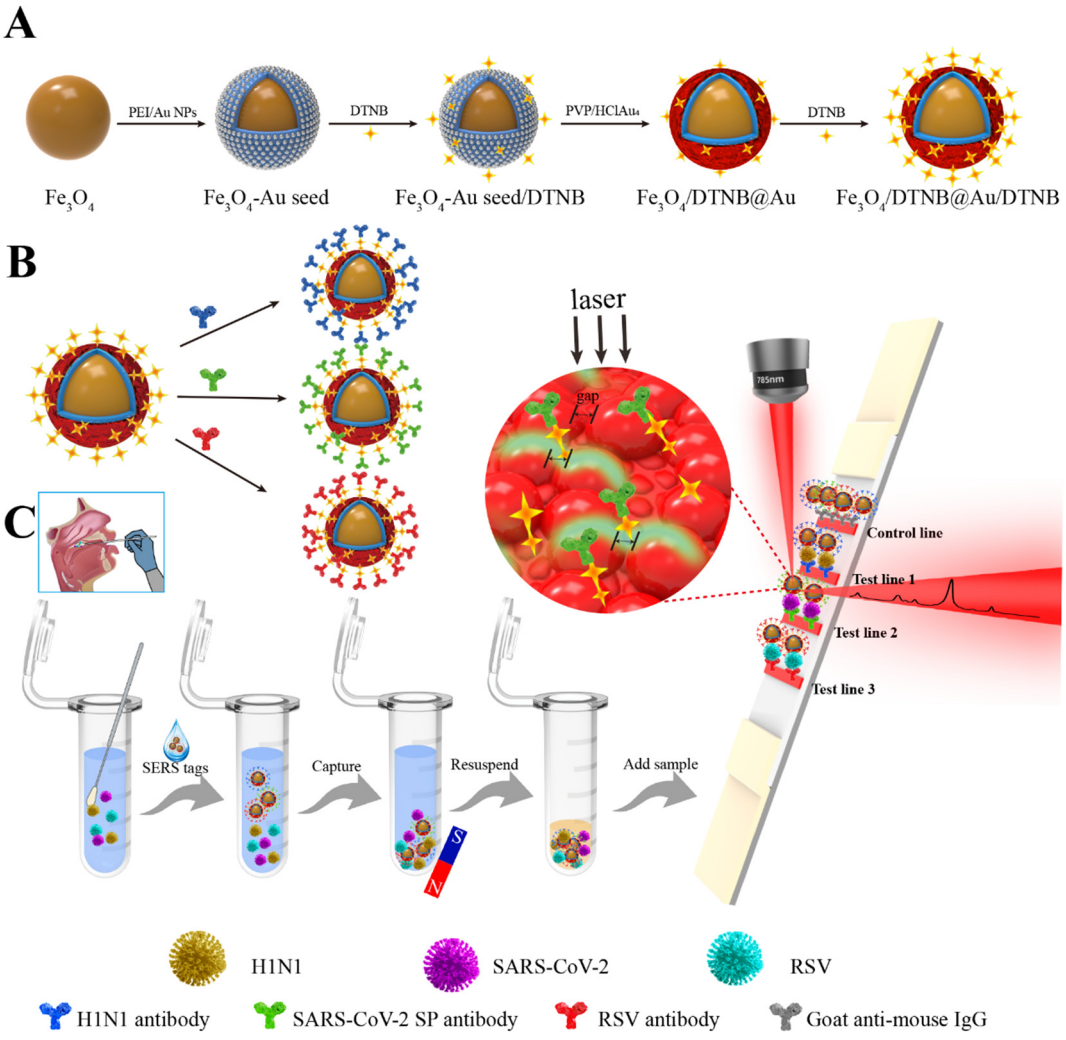

Scheme 1. Schematic of multichannel magnetic SERS-based LFA strip for the quantitative detection of respiratory viruses. (A) Synthesis of dual-layer DTNB-modified Fe_3O_4@Au MNPs. (B) Preparation of antibody-conjugated SERS tags for three respiratory viruses. (C) Collection of throat swab sample and operating procedure for the simultaneous quantitative detection of three respiratory viruses via the Fe_3O_4@Au-based SERS LFA strip.

Synthesis of immuno-Fe_3O_4@Au nanotags for magnetic SERS-based strip

As illustrated in Scheme. 1B, dual-layer DTNB-modified Fe_3O_4@Au MNPs were coupled with the anti-H1N1/SARS-CoV-2/RSV antibody by amidation reaction. Briefly, 1 mL of Fe_3O_4@Au MNPs modified with dual-layer DTNB were washed by deionized water and resuspended with 500 μL of MES buffer (10 mM, pH 5.5). Next, mixed EDC/NHS reagents (1 mM/2 mM) were added to activate the material by sonicating for 10 min. Then, activated Fe_3O_4@Au MNPs were gathered by the magnet, resuspended with 200 μL of 10 mM PBST (pH 7.4, 0.05 % Tween-20), and incubated with 10 μg of anti-H1N1/SARS-CoV-2/RSV antibody for 2 h with vigorous stirring at temperature. The excess carboxyl sites of immuno-Fe_3O_4@Au MNPs were blocked by 100 μL of 10 % BSA. Finally, immuno-Fe_3O_4@Au nanotags were magnetically washed with 10 mM PBST and resuspended into 200 μL of preservation solution (10 mM PBS containing 0.5 % sucrose, 0.5 % BSA, and 0.02 % NaN_3) as magnetic SERS tags for the detection of respiratory viruses.

Preparation of multichannel magnetic SERS-based LFA strip

Our multichannel magnetic SERS-based LFA strips consisting of a sample pad, an absorbent pad, and NC membrane with one control (C) and three T lines were able to detect three respiratory viruses, including H1N1, SARS-CoV-2, and RSV simultaneously. The antibodies sprayed on the top-to-bottom NC membrane were goat anti-mouse IgG (0.8 mg mL^{-1}), H1N1 (0.8 mg mL^{-1}), SARS-CoV-2 (0.8 mg mL^{-1}), and RSV (1 mg mL^{-1}) sequentially by the Biodot XYZ3050 plotter at a jetting rate of 0.1 μL mm^{-1}, namely, C line, T lines 1 (T_1), 2 (T_2), and 3 (T_3). The antibody-modified NC membrane was then dried in a thermostatic dryer at 37 °C for at least 2 h. Then, the PVC bottom plate assembled with the sample pad, NC membrane, and absorbent pad in sequence was cut into 3.0 mm wide strips and stored in a desiccator.

Simultaneous detection of respiratory viruses via the dual-layer DTNB Fe_3O_4@Au-LFA strips

Throat swabs from healthy people were immersed in 1 mL of buffer and spiked with a series of different concentrations of quantified inactivated H1N1 viruses, SARS-CoV-2 spike protein (SP), and RSV protein to simulate actual samples. In brief, 1 mL of prepared sample was incubated with 1.5 μL of three immuno-Fe_3O_4@Au nanotags and vigorously shaken for 15 min at room temperature. Next, immuno-Fe_3O_4@Au-H1N1/SARS-CoV-2/RSV complexes were enriched by magnet, resuspended in 75 μL of running solution (10 mM PBS containing 1 % Tween 20 and 5 % BSA), and then dropped onto the sample pad of the prepared LFA strip. After 15 min, the SERS signals on three T lines were captured and measured by a portable Raman system with a power of 10 mW for 5 s and 785 nm excitation.

Enzyme-linked immunosorbent assay

According to manufacturer's instructions of commercial ELISA kits, a series of gradient dilution virus samples were prepared, including inactivated H1N1 viruses, SARS-CoV-2 spike protein and RSV. After incubation, marker, color and etc., the optical density (OD) values of different microplate wells were detected by a microplate reader at 450 nm. Each group was assigned three independently repeated experiments. In addition, we simultaneously detected the inactivated H1N1 virus solution diluted 1000 times and different concentrations of Influenza H1N1 Hemagglutinin / HA recombinant protein supplied by the ELISA kit. The measured OD values and corresponding concentrations of H1N1 recombinant protein were used to plot standard curve by Origin 8.5.0 software and calculated the original concentration of H1N1 virus solution.

Results and discussion

Operating principle of multichannel magnetic SERS-based LFA for the simultaneous detection of three respiratory viruses

We developed a multichannel magnetic SERS-based LFA strips that could efficiently and specifically identify three different respiratory viruses simultaneously. As shown in Scheme 1, the testing principle of Fe_3O_4@Au-LFA strips were based on specific antigen–antibody reaction for the simultaneous and quantitative detection of H1N1, SARS-CoV-2, and RSV in throat swab samples.[36] To achieve high sensitivity and specificity for detection, we synthesized the dual-layer DTNB-modified immuno-Fe_3O_4@Au nanotags with the following advantages. (i) Fe_3O_4 (~220 nm) served as the core offered huge surface and abundant carboxyl sites, which could capture and enrich maximum target viruses from complex samples rapidly. (ii) The dual-layer DTNB-modified Fe_3O_4@Au MNPs offered approximately three times stronger SERS signals than the monolayer. (iii) Au shell coated on the surface of Fe_3O_4 MNPs was of strong stability and oxidation resistance.

The quantitative detection of three respiratory viruses could be achieved through the following process (Scheme 1C). First, the samples on the swab were immersed in 1 mL of diluent and added with antibody-conjugated Fe_3O_4@Au nanotags to recognize and capture H1N1/SARS-CoV-2/RSV. After incubation, the formed Fe_3O_4@Au-antibody-H1N1/SARS-CoV-2/RSV immune complexes were magnetically gathered and resuspended in the running buffer. Next, the above buffer was loaded onto the sample pad and then migrated by capillary action toward the absorbent pad of the strip. The detection antibodies of respiratory viruses precoated on T lines specifically conjugated corresponding target viruses due to the antigen–antibody reaction. Redundant Fe_3O_4@Au nanotags without conjugating viruses continued to migrate along the strips and captured by the antibody precoated on the C line. According to the principle of localized surface plasmon resonance, the molecule of DTNB absorbed on the Fe_3O_4@Au nanotags greatly amplified its SERS intensity by the hot spots generated by the gap of Au particles.[37] Moreover, increased viruses in the sample resulted in increased Fe_3O_4@Au nanotags intercepted on the T line and strong SERS signals of the T line. Therefore, the accurate quantitative detection of these three viruses could be realized by detecting SERS signals of three T lines. Finally, the measurement of SERS signals of the three T lines for H1N1, SARS-CoV-2, and RSV were performed using a portable Raman system. When added the sample, the C line of the strip visualized indicating that the strip was valid and the T_1, T_2, or T_3 colored when even one respiratory virus, such as H1N1, SARS-CoV-2, or RSV, was present in the sample. However, three T lines and C line colored if the sample simultaneously had three target viruses. On the basis of this experimental principle, our proposed magnetic SERS-based strip could simultaneously and ultrasensitively detect different concentrations of three kinds of respiratory viruses in the sample by measuring the SERS signals corresponding to T lines.

Preparation and characterization of Fe_3O_4@Au SERS MNPs

The preparation process of dual-layer DTNB-modified Fe_3O_4@Au MNPs by a previously reported PEI-mediated seed growth method[38] is illustrated in Scheme 1A. The images of high-resolution transmission electron microscope (HR-TEM) and scanning electron microscopic (SEM) in Fig. 1A-C and D-F, respectively, displayed the morphology of Fe_3O_4@Au MNPs at different stages. Obviously, theses composite MNPs were spherical, uniform particle size, and monodispersed. Moreover, small Au NPs were adsorbed densely onto the surface of Fe_3O_4 MNPs and acted as nucleation sites for the subsequent synthesis of the Au shell. And the mean diameter of Fe_3O_4 MNPs grew from 220 nm to 290 nm after Au shell was coated. Furthermore, the energy dispersive spectroscopy element mapping (Fig. 1D) further confirmed the elemental composition of Fe_3O_4@Au MNPs, in which the magnetic core consisting of Fe (green) and O (blue) was densely surrounded with masses of Au NPs (red). The UV–vis spectra of materials at different phases were obtained by a UV–vis spectrometer in deionized water (Fig. S1A). The absorption of small Au NPs did not influence the UV–vis spectra of Fe_3O_4, whereas the absorption peaks of Fe_3O_4@Au MNPs evidently red-shifted, and the peak intensity was higher. Furthermore, the DTNB modified onto the surface of Fe_3O_4-Au seed and Fe_3O_4@Au MNPs slightly changed the absorption curves. This surface plasmon coupling phenomenon was because of the formation of dense and rough Au shell. Additionally, the

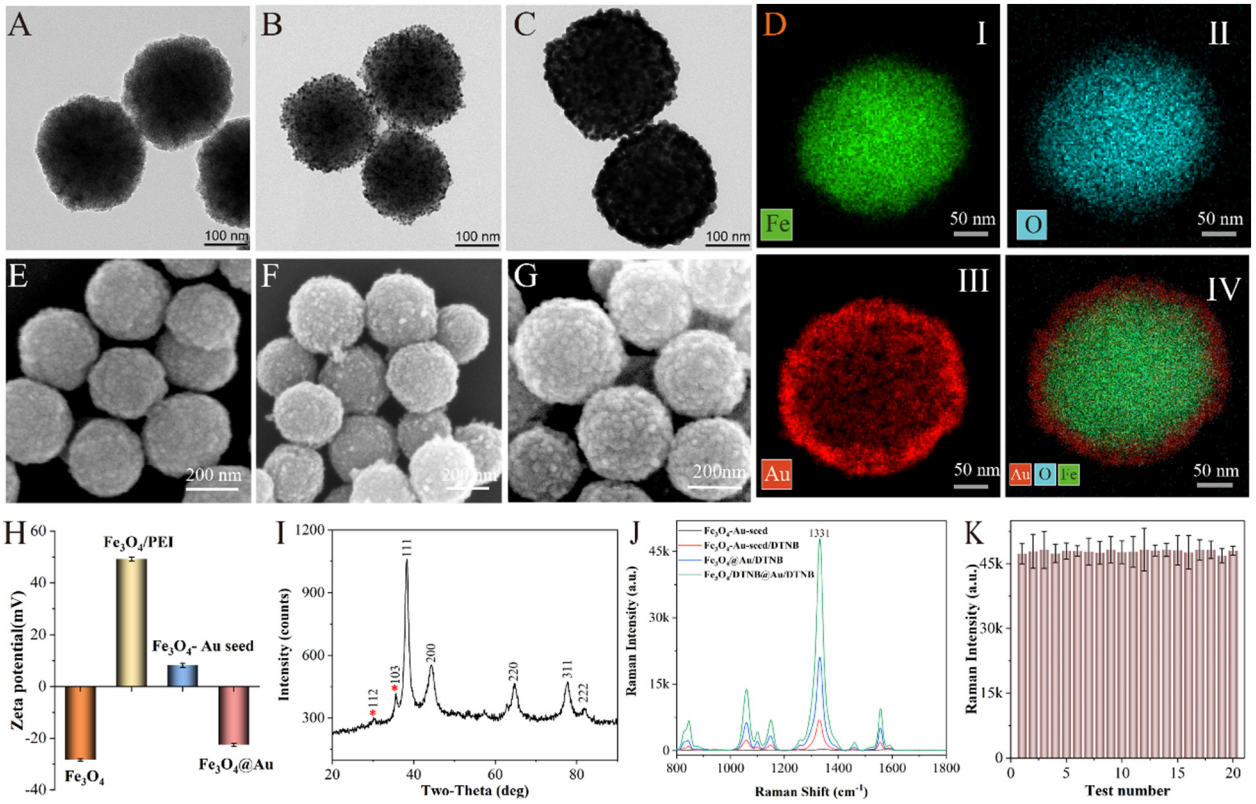

Fig. 1. Characterization of the prepared Fe_3O_4@Au MNPs. HR-TEM images of (A) Fe_3O_4 MNPs, (B) Fe_3O_4-Au seed MNPs, (C) Fe_3O_4@Au MNPs, and (*E*-G) their corresponding SEM images. (D) Elemental mapping images of Fe_3O_4@Au MNPs. (H) Zeta potential of the as-obtained samples during different stages. (I) XRD pattern of Fe_3O_4@Au MNPs. (J)SERS spectra of Fe_3O_4-Au seed, Fe_3O_4-Au seed/DTNB, Fe_3O_4@Au/DTNB, and Fe_3O_4/DTNB@Au/DTNB MNPs under the same condition. (K) SERS intensities of Fe_3O_4@Au MNPs at 1331 cm^{-1} detected 20 times in four different batches.

zeta potential of the obtained samples during different stages in the synthesis of Fe_3O_4@Au MNPs was investigated and measured in distilled water (Fig. 1H). The increased potential was due to the PEI layer with strong positive charge, and the decreased potential was driven by the Au shell with negative charge. Such regular and stable variation in potentials exactly confirmed that the synthetic method of Fe_3O_4@Au MNPs was driven by electrostatic adsorption. Notably, the zeta potential decreased after the DTNB modified on to the seeds and Fe_3O_4@Au MNPs since the DTNB was negatively charged (Fig. S1B). In addition, the X-ray diffraction (XRD) pattern of Fe_3O_4@Au MNPs showed in Fig. 1I also confirmed successful formation of the Au shell. And the diffraction peaks of the as-prepared Fe_3O_4@Au MNPs can be indexed to the corresponding Powder Diffraction File (PDF) database (PDF 75–1609 for Fe_3O_4 and 04–0784 for Au). More specifically, the peaks of curve can be observed at 2θ values of 30.1 and 35.5 which correspond to the reflections of the 112 and 103 crystalline planes of the synthesized Fe_3O_4 MNPs, respectively. Furthermore, the peaks of curve at 2θ values of 38.1, 44.3, 64.5, 77.5 and 81.7 were corresponded to the reflections of the 111, 200, 220, 311 and 222 crystalline planes of the synthesized Au shell, respectively. The Au coated on Fe_3O_4 MNPs can produce electromagnetic enhancement through surface plasmon resonance to enhance the Raman signal of molecular on the substrate. Besides, the X-ray photoelectron spectroscopy (XPS) patterns shown in Fig. S2A revealed that characteristic peaks of Au appeared at 83.3 eV (Au4f), 109.1 eV (Au5s), 335 eV (Au4d5), 353 eV (Au4d3), 546.1 eV (Au4p3), 642.1 eV (Au4p1), and 762.1 eV (Au4s) after the formation of Au shell. Moreover, the magnetic hysteresis curves (Fig. S2B) showed good superparamagnetism and the magnetization saturation (MS) values of Fe_3O_4 and Fe_3O_4@Au MNPs were 68.89 and 21.01 emu g^{-1}, respectively. The decrease of MS value after the formation of Au shell indicated the increased nonmagnetic components. On this basis, Fe_3O_4@Au MNPs could be applied for the rapid enrichment and separation of targets from complex samples.

SERS performance of Fe_3O_4@Au magnetic nanotags

The Raman reporter molecule, namely DTNB, served as the bridge connecting the Au shell and the capture antibody. The double sulfur bond of DTNB can spontaneously form a stable Au—S bond between DTNB and Fe_3O_4@Au MNPs, and the free carboxyl of DTNB can bind the antibody by the condensation reaction.[39] Moreover, the Raman signal intensity at the main peak (1331 cm^{-1}) of DTNB varied significantly with the change in concentrations and could be used for quantitative detection. The SERS properties of Fe_3O_4@Au MNPs were assessed as follows. By optimizing the concentration of DTNB modified on 1 mg mL^{-1} of Fe_3O_4-Au seeds and corresponding Fe_3O_4@Au MNPs (Fig. S3), 80 μM of DTNB solution made

them saturated and SERS signals reached the highest. Furthermore, Fe_3O_4-Au seed without DTNB had no Raman peak, whereas Fe_3O_4-Au seed with DTNB had lower SERS intensity than Fe_3O_4@Au/DTNB at 1331 cm^{-1} (Fig. 1J). Furthermore, the SERS intensity of Fe_3O_4/DTNB@Au /DTNB was roughly three times stronger than that of the single layer due to the inner layer of DTNB molecules and hotspots on the surface of the Au shell. And the SERS enhancement factor (EF) value of the peak at 1331 cm^{-1} for DTNB was estimated to be 2.61×10^6 approximately by the adjustive method, as detailed in Supporting Information S4. We also investigated the SERS intensity at 1331 cm^{-1} of the dual-layer DTNB-modified Fe_3O_4@Au MNPs by detection for 20 times in four different batches (Fig. 1K). Results confirmed the high reproducibility and excellent stability between and within batches. Moreover, Fe_3O_4@Au MNPs showed unchanging SERS intensities in ethanol during 60 days and high SERS intensity in water solution at pH 8–14 (Figs. S4-S5). With the excellent SERS properties and stability, the dual-layer DTNB Fe_3O_4@Au MNPs modified as immune tags can deal with complex samples.

Optimization of Fe_3O_4@Au-based SERS strips

For the ultrasensitive and simultaneous detection of respiratory viruses via Fe_3O_4@Au SERS nanotags, several key conditions during the detection process should be optimized, and optimization results were as illustrated in Figs. S6–S8 (Supporting Information). The concentration of the detection antibody on the T line should be enough to capture the antigen–antibody–tag immunocomplex and avoid nonspecific conjugation. As shown in Fig. S6, the ideal concentrations of H1N1, SARS-CoV-2, and RSV detection antibodies sprayed onto T lines were 0.8, 0.8, and 1 mg mL^{-1}, respectively, whereas the signal-to-noise ratio (SNR) was highest or the appropriate choose. Likewise, the optimal composition of running buffer was 5 % BSA and 1 % Tween-20 added in 10 mM PBS (Fig. S7). Moreover, 10 min of incubation time and 15 min of reaction time were enough for the formation of tags-virus immunocomplex in the sample and conjugation with detecting antibodies on the strips (Fig. S8).

Performance estimation of Fe_3O_4@Au-based SERS strips

On the basis of above optimized experiments, the multichannel magnetic SERS-based LFA was established for the simultaneous detection of three respiratory viruses and evaluated by simultaneously detecting H1N1, SARS-CoV-2, and RSV under the same conditions. A series of tests with different concentrations of H1N1, SARS-CoV-2, RSV, and other associated viruses were carried out to confirm the detection capability of our proposed method. As shown in Fig. 2A, the magnetic SERS-based LFA strip displayed three black T lines while the sample with H1N1/SARS-CoV-2/RSV, and the black T lines disappeared while the corresponded antigen was absent in the sample. Evidently, no cross-reaction was observed among three T lines for these target respiratory viruses. Furthermore, the SERS intensities of T lines corresponding to the strips were then measured by a portable Raman spectrometer (Fig. 2A). Apparently, the color and the SERS intensity of T_1 for H1N1 were darker and higher than those of T_2 for SARS-CoV-2 and T_3 for RSV. This phenomenon was intelligible because the affinity between different antibodies and antigens varied. A strong affinity of the detection antibody increased the Fe_3O_4@Au nanotags remained on the T line. Therefore, among three anti-H1N1/SARS-CoV-2/RSV antibodies, the affinity of the monoclonal anti-H1N1 antibody was considered strongest.

Various common respiratory viruses, such as MERS (100 ng mL^{-1}), Flu B (10^8 copies mL^{-1}), and HAdV (10^6 pfu mL^{-1}), were selected as nonspecific viruses to confirm the specificity of

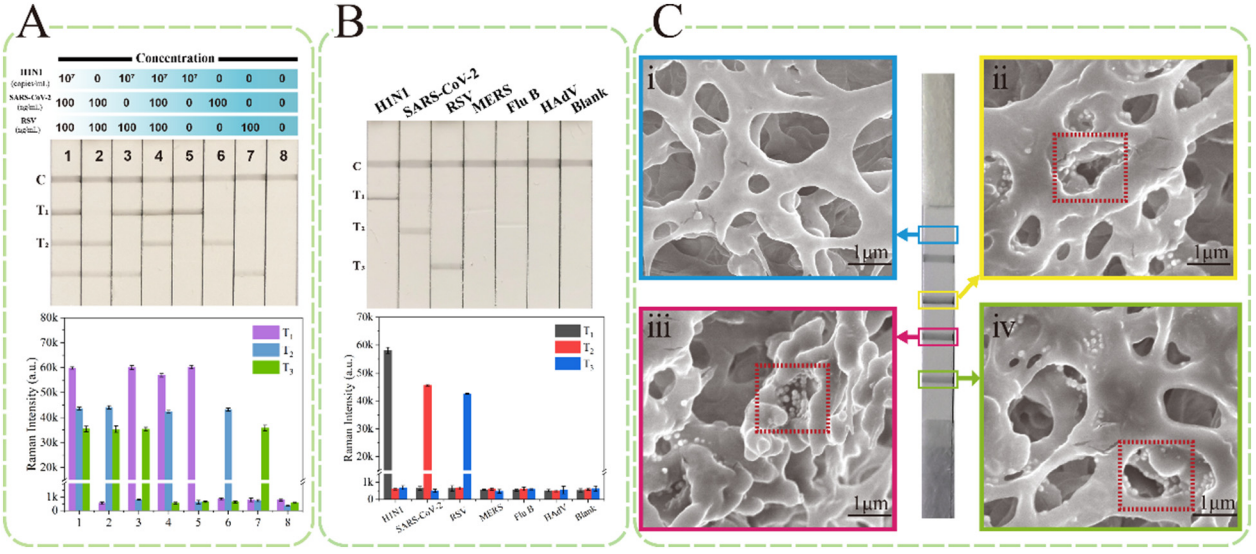

Fig. 2. (A) Photographs and corresponding SERS intensity at 1331 cm^{-1} of the proposed strips with different concentration of H1N1, SARS-CoV-2 and RSV. (B) Photographs and corresponding SERS intensity at 1331 cm^{-1} of specificity experiments via the Fe_3O_4@Au-based SERS strips. Error bars are calculated from five measurements. (C) SEM images of the (i) NC membrane and SERS-based LFA strips in the presence of (ii) 10^7 copies mL^{-1} of H1N1, (iii) 100 ng mL^{-1} of SARS-CoV-2, and (iv) 100 ng mL^{-1} of RSV.

the magnetic SERS-based LFA strip. Target viruses, including 10^7 copies mL^{-1} of H1N1 and 100 ng mL^{-1} of SARS-CoV-2 SP and RSV, were also prepared. As shown in Fig. 2B, target viruses consisting of H1N1, SARS-CoV-2, and RSV displayed a distinct black band and high SERS intensities on their corresponding T lines of the strips, whereas nontarget viruses only showed black C line and less than 1000 a.u. of the SERS intensity of all the other T lines. Detection results confirmed that our proposed magnetic SERS-based LFA strip possessed remarkable specificity and could specifically identify H1N1/SARS-CoV-2/RSV from other familiar respiratory viruses, which induced similar respiratory symptoms. Fig. 2C i) shows the SEM image of NC membrane, and Fig. 2C ii–iv) show T_1, T_2, and T_3 lines, respectively, on SERS-based LFA strips. No visible Fe_3O_4@Au MNPs was adsorbed on the nondetecting line of the strip, whereas many Fe_3O_4@Au tags were captured by antibodies sprayed on the corresponding T line as the sample with target viruses.

In summary, our proposed Fe_3O_4@Au-based SERS strips could be efficiently used to detect the target respiratory viruses quantitatively by measuring the SERS signals of the corresponding three T lines at one time. In addition, different concentrations of viruses were added into the sample, and five repetitive tests per group were carried out to ensure the stability of the magnetic SERS-based LFA strip (Fig. S9). All tested SERS-based LFA strips exhibited remarkable reproducibility of SERS signals on three T lines because the relative standard deviation (RSD) values were no more than 10 %.

Sensitivity analysis of the multichannel Fe_3O_4@Au-SERS-based LFA

The sensitivity and quantitative ability of this method were investigated by detecting different concentrations of H1N1/SARS-CoV-2/RSV in throat swab samples. Fig. 3A and B show the pictures of the testing strips by Fe_3O_4@Au-LFA and Au NP-LFA, respectively, with the same pairs of antibodies, and the visual limits of both methods for H1N1, SARS-CoV-2, and RSV were 10^4 copies mL^{-1}, 1 ng mL^{-1}, and 1 ng mL^{-1}, respectively. Au NP-LFA strips were prepared as illustrated in Supporting Information. Furthermore, Fig. 3A demonstrates that the mapping images of the SERS intensity at 1331 cm^{-1} corresponded to the T lines of the tested strips for different concentrations of target viruses. SERS maps were obtained by measuring 128 points in the rectangle area of the T lines by a Renishaw invia plus Raman system, and the detecting step was set as 20 × 20 μm. Quantitative detection was implemented by measuring the SERS signals of the immune Fe_3O_4@Au SERS nanotags captured onto the T line. The SERS spectra shown in Fig. 3C–E corresponded to the T lines of the SERS strips in Fig. 3A, revealing that the SERS intensity became strong with increasing concentration of corresponded viruses. Moreover, the SERS intensities at 1331 cm^{-1} of T lines were used to plot the calibration curves of H1N1, SARS-CoV-2 SP, and RSV (Fig. 3F–H). The limit of detection (LOD) of SERS-based LFA was stipulated using the International Union of Pure and Applied Chemistry (IUPAC) protocol: $LOD = y_{blank} + 3\ SD_{blank}$, where y_{blank} represents the average SERS intensity at 1331 cm^{-1}, and SD_{blank} is the standard deviation of the blank control. Therefore, the LODs for H1N1, SARS-CoV-2, and RSV detection were 85 copies mL^{-1}, 8 pg mL^{-1}, and 8 pg mL^{-1}, respectively. Thus, the sensitivity of the magnetic SERS-based LFA was 100 times higher than that of the colloidal Au-LFA. Moreover, the SERS intensities of T_{1-3} for H1N1/SARS-CoV-2/RSV displayed wide dynamic relationships with the concentrations of three target viruses, and the values of R^2 were more than 0.98 (Fig. 3F–H). These results showed the ultrasensitive and quantitative detection ability of the Fe_3O_4@Au-LFA for target respiratory viruses. In addition, we compared our fabricated SERS sensor and other recently reported sensors for H1N1/SARS-CoV-2/RSV detection as shown in Table S1. Obviously, the essential factors for detection of our proposed magnetic Fe_3O_4@Au-SERS LFA surpassed most of them, reflecting in multi-channel, sensitivity, and detecting time.

Respiratory virus detection in throat swab samples

To further evaluate the repeatability and precision of our method, we detected a series of different concentrations of H1N1 virions (10^6–10^4 copies mL^{-1}), SARS-CoV-2 SP (10–0.1 ng mL^{-1}), and RSV (10–0.1 ng mL^{-1}) spiked in throat swab samples via Fe_3O_4@Au-LFA strips. As summarized in Table 1, the average recovery values of spiked target viruses were 93.2 % to 127 % with relatively low coefficients of variation (CV) values ranging from 1.71 % to 6.25 %. These results were obtained from three separate tests and exhibited acceptable repeatability and precision of our proposed assay for the quantification of target viruses.

Sensitivity detection via ELISA

The mature method, such as commercial ELISA kits, was used to detect these three target respiratory viruses and further verify the detecting properties of the Fe_3O_4@Au-LFA strip. Results are shown in Fig. S10. By analyzing the OD_{450} values of different microplate wells, the LODs detected by ELISA for H1N1, SARS-CoV-2, and RSV were 5 × 10^4 copies mL^{-1}, 0.05 ng mL^{-1}, and 5 ng mL^{-1}, respectively. Thus, the sensitivity values of the magnetic Fe_3O_4@Au-LFA strip for H1N1, SARS-CoV-2, and RSV detection were higher than that of ELISA by 500, 5, and 500 times, respectively. Furthermore, the inactive H1N1 virus solution diluted 1000 times was calculated to be 498 pg mL^{-1} based on the standard curve of H1N1 recombinant protein. The original concentration of H1N1 virus solution (10^9 copies mL^{-1}) was correspondingly converted to 498 ng mL^{-1} and the LOD for H1N1 detected by our magnetic SERS-LFA was 0.04 pg mL^{-1} (85 copies mL^{-1}). Notably, the ratio between the number of viral antigens (HA) and the RNA copy numbers can vary widely between virions and treatments. Accordingly, these ratios should not be considered absolute but only provide a relative comparison between the assays. In addition, ELISA took approximately 4 h, whereas our method was finished within 30 min and did not need skilled personnel, revealing that the Fe_3O_4@Au-based SERS strip was appropriate for the simultaneously rapid and quantitative detection of clinical samples.

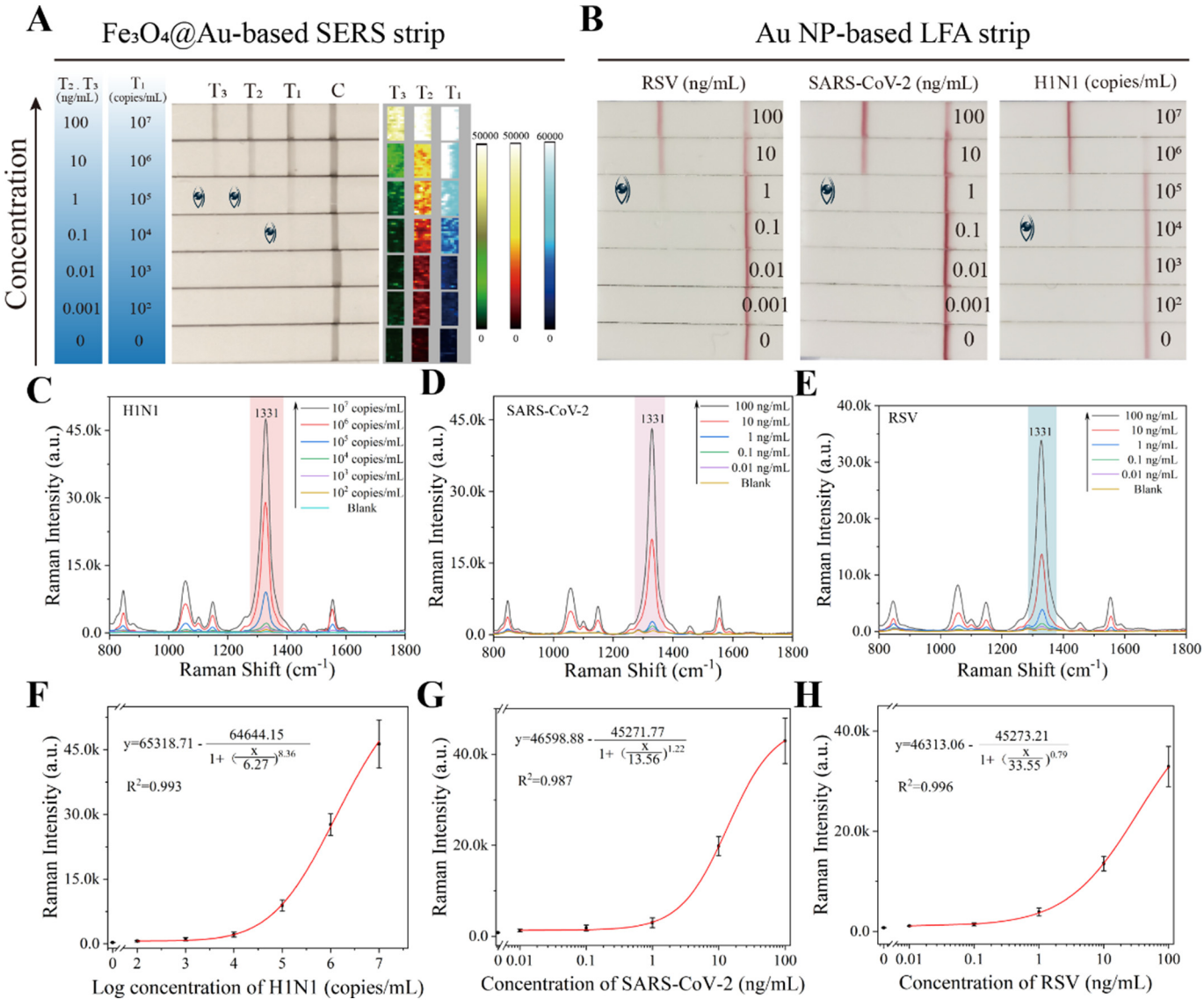

Fig. 3. (A) Photographs of Fe_3O_4@Au-based SERS strips and corresponding SERS mapping images of three T lines for different concentrations of H1N1, SARS-CoV-2, and RSV. (B) Photographs of Au NP-based LFA strips for H1N1, SARS-CoV-2, and RSV detection. (C-E) Average SERS spectra of three T lines for different concentrations of H1N1, SARS-CoV-2, and RSV. (F—H) Corresponding calibration curves of H1N1, SARS-CoV-2, and RSV with SERS intensities at 1331 cm^{-1}. Error bars indicate the standard deviations measured from three separate experiments.

Table 1
Recovery results for H1N1, SARS-CoV-2 SP, and RSV virions spiked in throat swab samples.

Target	Added concentration	Detected concentration	Recovery (%)	CV (%, n = 3)
H1N1 (log copies mL^{-1})	6	5.8	96.6	2.48
	5	5.1	102	3.11
	4	4.3	107.5	5.41
SARS-CoV-2 SP (ng mL^{-1})	10	9.32	93.2	2.41
	1	1.05	105	2.42
	0.1	0.11	110	6.10
RSV (ng mL^{-1})	10	11.18	111.8	1.71
	1	1.27	127	6.25
	0.1	0.097	97	3.71

Sensitivity detection of inactivated viruses by Fe_3O_4@Au-SERS LFA strips

Given that all experiments conducted before detected the purified proteins of SARS-CoV-2 SP and RSV, we also examined the inactivated viruses of SARS-CoV-2 and RSV for practical clinical sample via the multichannel Fe_3O_4@Au-based SERS LFA. And the visual testing results were 10^5 copies mL^{-1} and 10^3 $TCID_{50}$ mL^{-1} for inactivated SARS-CoV-2 (Fig. 4A) and RSV virions (Fig. 4B), respectively. Fig. 4A (ii) and (iii) exhibit the SERS spectra and intensities at 1331 cm^{-1} of the T_2 for a series of concentrations of inactivated SARS-CoV-2, respectively, and the LOD of our method for inactivated SARS-CoV-2 virions was 10^3 copies mL^{-1} by calculating. Likewise, the LOD for inactivated RSV virions were 8 $TCID_{50}$ mL^{-1} by analyzing the SERS signals

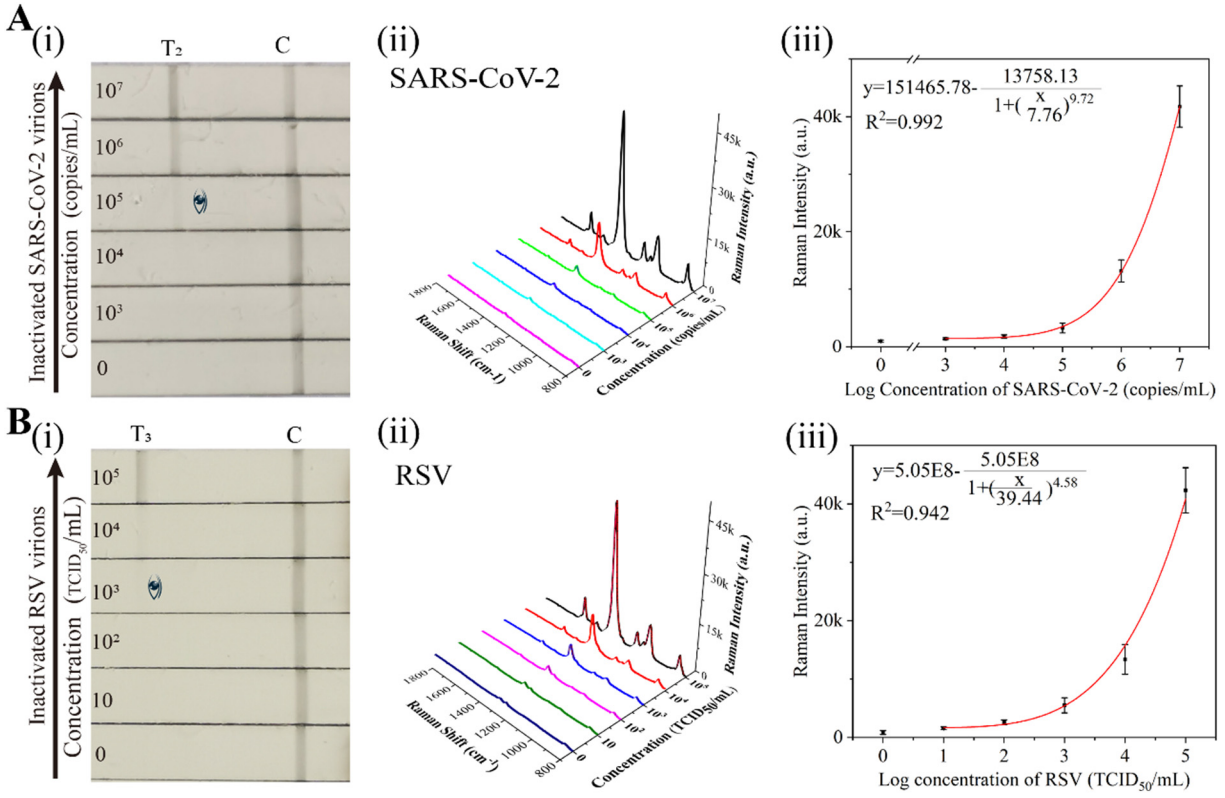

Fig. 4. Photographs of Fe_3O_4@Au-based SERS strips and corresponding SERS signals of T lines for different concentrations of (A) inactivated SARS-CoV-2 and (B) RSV virions. Error bars are calculated from three independent measurements.

of T_3 for a series of concentrations of inactivated RSV shown in Fig. 4B (ii) and (iii). These results revealed the high sensitivity of the multichannel Fe_3O_4@Au-SERS LFA for detecting real SARS-CoV-2 and RSV virions.

Conclusion

In this study, we reported a multichannel magnetic SERS-based LFA for the ultrasensitive and simultaneous detection of respiratory viruses, including H1N1, SARS-CoV-2 and RSV. High-performance Fe_3O_4@Au MNPs (220 nm) were prepared with high monodispersity and strong ability of SERS enhancement. Moreover, the dual layer of DTNB modified onto the big core of Fe_3O_4@Au MNPs provided strong SERS signals and abundant conjugated sites for specific antibodies. The as-prepared Fe_3O_4@Au nanotags with three different capture antibodies of viruses could specifically capture and magnetically enrich the H1N1/SARS-CoV-2/RSV removing the impurities from throat swab samples, and these three viruses were quantitatively detected by analyzing SERS signals on the corresponding T lines. The LODs of the proposed Fe_3O_4@Au-based SERS strips arrived at 85 copies mL^{-1}, 8 pg mL^{-1}, and 8 pg mL^{-1} for H1N1, SARS-CoV-2 and RSV, respectively, revealing that the sensitivity of our method was improved by 100 and 5–500 times than those of colloidal Au NP-LFA and ELISA, respectively. Furthermore, our method's great specificity, reproducibility, and detection of real respiratory viruses in throat swab samples were proven. To our knowledge, this work first established a multichannel SERS-based LFA for the simultaneous detection of three respiratory viruses, namely, H1N1, SARS-CoV-2 and RSV. Thus, the proposed method had remarkable potentials as a diagnostic platform for the rapid and accurate detection of respiratory viruses under field conditions.

CRediT authorship contribution statement

Zhenzhen Liu: Methodology, Visualization, Writing – original draft, Writing – review & editing. **Chongwen Wang:** Conceptualization, Methodology. **Shuai Zheng:** Methodology, Visualization. **Xingsheng Yang:** Methodology. **Han Han:** Methodology. **Yuwei Dai:** Methodology. **Rui Xiao:** Conceptualization, Writing – review & editing, Supervision.

Declaration of competing interest

We declare that this manuscript has no any commercial or associative interest, current and within the past five years, that might pose a potential, perceived or real conflict of interest. These include grants, patent licensing arrangements, consultancies, stock or other equity ownership, advisory board memberships, or payments for conducting or publicizing the study. The study was supported by the National Key Research and Development Program of China (2021YFC2301102), the Major Project (BWS18J008, JK20202A060431), and Youth Cultivation Project (21QNPY151).

Appendix A. Supplementary data

Supplementary data to this article can be found online at https://doi.org/10.1016/j.nano.2022.102624.

References

1. Wylie KM. The virome of the human respiratory tract. *Clin Chest Med* 2017;**38**:11-9.
2. WHO. Weekly epidemiological update on COVID-19 - 20 April 2022 Available at www.who.int/publications/m/item/weekly-epidemiological-update-on-covid-19—20-april-2022.
3. Dao TL, Hoang VT, Colson P, Million M, Gautret P. Co-infection of SARS-CoV-2 and influenza viruses: a systematic review and meta-analysis. *JClinVirolPlus* 2021:1.
4. Hazra A, Collison M, Pisano J, Kumar M, Oehler C, Ridgway JP. Coinfections with SARS-CoV-2 and other respiratory pathogens. *Infect Control Hosp Epidemiol* 2020;**41**:1228-9.
5. Zhang NN, Li XF, Deng YQ, Zhao H, Huang YJ, Yang G, et al. A thermostable mRNA vaccine against COVID-19. *Cell* 2020;**182**(1271–1283)e16.
6. Li J, Lin R, Yang Y, Zhao R, Song S, Zhou Y, et al. Multichannel immunosensor platform for the rapid detection of SARS-CoV-2 and influenza A (H1N1) virus. *ACS Appl Mater Interfaces* 2021;**13**:22262-70.
7. Vemula SV, Zhao J, Liu J, Wang X, Biswas S, Hewlett I. Current approaches for diagnosis of influenza virus infections in humans. *Viruses* 2016:8.
8. Augustine R, Hasan A, Das S, Ahmed R, Mori Y, Notomi T, et al. Loop-mediated isothermal amplification (LAMP): a rapid, sensitive, specific, and cost-effective point-of-care test for coronaviruses in the context of COVID-19 pandemic. *Biology* 2020:9 (Basel).
9. Lin Y, Jingyao W, Xuelong L, Lingling M, Yi S, Weihua C, et al. Simultaneous detection of SARS-CoV-2 and pandemic (H1N1) 2009 virus with real-time isothermal platform. *Heliyon* 2021;**7**.
10. Liu Y, Tan Y, Fu Q, Lin M, He J, He S, et al. Reciprocating-flowing on-a-chip enables ultra-fast immunobinding for multiplexed rapid ELISA detection of SARS-CoV-2 antibody. *BiosensBioelectro* 2021;**176**.
11. Peng R, Pan Y, Li Z, Qin Z, Rini JM, Liu X. SPEEDS: a portable serological testing platform for rapid electrochemical detection of SARS-CoV-2 antibodies. *Biosens Bioelectron* 2021;**197**113762.
12. Jia X, Liu Z, Peng Y, Hou G, Chen W, Xiao R. Automatic and sensitive detection of West Nile virus non-structural protein 1 with a portable SERS-LFIA detector. *Mikrochim Acta* 2021;**188**:206.
13. Yin X, Dou L, Hu H, Du T, Liu S, Zhao M, et al. An immune-scaffold relying biosensor for simultaneous detection of nitrofurazone and furazolidone. *Sensors Actuators B Chem* 2021;**345**.
14. Xiaokun W, Namhyun C, Ziyi C, Juhui K, Lingxin C, Jaebum C. Simultaneous detection of dual nucleic acids using a SERS-based lateral flow assay biosensor. *Anal Chem* 2017;**89**.
15. Huang Z, Zhang A, Zhang Q, Cui D. Nanomaterial-based SERS sensing technology for biomedical application. *J Mater Chem B* 2019;**7**:3755-74.
16. Pang Y, Li Q, Wang C, Zhen S, Sun Z, Xiao R. CRISPR-cas12a mediated SERS lateral flow assay for amplification-free detection of double-stranded DNA and single-base mutation. *ChemEngJ* 2022;**429**.
17. Feliu N, Hassan M, Garcia Rico E, Cui D, Parak W, Alvarez-Puebla R. SERS quantification and characterization of proteins and other biomolecules. *Langmuir* 2017;**33**:9711-30.
18. Karakus E, Erdemir E, Demirbilek N, Liv L. Colorimetric and electrochemical detection of SARS-CoV-2 spike antigen with a gold nanoparticle-based biosensor. *Anal Chim Acta* 2021;**1182**338939.
19. Lin D, Qin T, Wang Y, Sun X, Chen L. Graphene oxide wrapped SERS tags: multifunctional platforms toward optical labeling, photothermal ablation of bacteria, and the monitoring of killing effect. *ACS Appl Mater Interfaces* 2014;**6**:1320-9.
20. Sun Y, Xu L, Zhang F, Song Z, Hu Y, Ji Y, et al. A promising magnetic SERS immunosensor for sensitive detection of avian influenza virus. *Biosens Bioelectron* 2017;**89**:906-12.
21. Wang C, Wang C, Wang X, Wang K, Zhu Y, Rong Z, et al. Magnetic SERS strip for sensitive and simultaneous detection of respiratory viruses. *ACS Appl Mater Interfaces* 2019;**11**:19495-505.
22. Pazos-Perez N, Guerrini L, Alvarez-Puebla RA. Plasmon tunability of gold nanostars at the tip apexes. *ACS Omega* 2018;**3**:17173-9.
23. Jia X, Wang C, Rong Z, Li J, Wang K, Qie Z, et al. Dual dye-loaded Au@Ag coupled to a lateral flow immunoassay for the accurate and sensitive detection of mycoplasma pneumoniae infection. *RSC Adv* 2018;**8**:21243-51.
24. Lu L, Yu J, Liu X, Yang X, Zhou Z, Jin Q, et al. Rapid, quantitative and ultra-sensitive detection of cancer biomarker by a SERRS-based lateral flow immunoassay using bovine serum albumin coated Au nanorods. *RSC Adv* 2020;**10**:271-81.
25. Wang J, Wu X, Wang C, Rong Z, Ding H, Li H, et al. Facile synthesis of Au-coated magnetic nanoparticles and their application in bacteria detection via a SERS method. *ACS Appl Mater Interfaces* 2016;**8**:19958-67.
26. Hwang J, Lee S, Choo J. Application of a SERS-based lateral flow immunoassay strip for the rapid and sensitive detection of staphylococcal enterotoxin B. *Nanoscale* 2016;**8**:11418-25.
27. Maneeprakorn W, Bamrungsap S, Apiwat C, Wiriyachaiporn N. Surface-enhanced Raman scattering based lateral flow immunochromatographic assay for sensitive influenza detection. *RSC Adv* 2016;**6**:112079-85.
28. Liu H, Dai E, Xiao R, Zhou Z, Zhang M, Bai Z, et al. Development of a SERS-based lateral flow immunoassay for rapid and ultra-sensitive detection of anti-SARS-CoV-2 IgM/IgG in clinical samples. *Sensors Actuators B Chem* 2021;**329**129196.
29. Fularz A, Almohammed S, Rice JH. Oxygen incorporation-induced SERS enhancement in silver nanoparticle-decorated ZnO nanowires. *ACS Appl-Nano Mater* 2020;**3**:1666-73.
30. Erol M, Han Y, Stanley SK, Stafford CM, Du H, Sukhishvili S. SERS not to be taken for granted in the presence of oxygen. *J Am Chem Soc* 2009;**131**:7480-1.
31. Sobczak-Kupiec A, Venkatesan J, Alhathal AlAnezi A, Walczyk D, Farooqi A, Malina D, et al. Magnetic nanomaterials and sensors for biological detection. *Nanomedicine* 2016;**12**:2459-73.
32. Bai Z, Wei H, Yang X, Zhu Y, Peng Y, Yang J, et al. Rapid enrichment and ultrasensitive detection of influenza a virus in human specimen using magnetic quantum dot nanobeads based test strips. *Sensors Actuators B Chem* 2020;**325**128780.
33. Srivastava A, Das R, Prajapati YK. Effect of perovskite material on performance of surface plasmon resonance biosensor. *IET Optoelectron* 2020;**14**:256-65.
34. Wang C, Wang J, Li M, Qu X, Zhang K, Rong Z, et al. A rapid SERS method for label-free bacteria detection using polyethylenimine-modified Au-coated magnetic microspheres and Au@Ag nanoparticles. *Analyst* 2016;**141**:6226-38.
35. Liu X, Yang X, Li K, Liu H, Xiao R, Wang W, et al. Fe3O4@Au SERS tags-based lateral flow assay for simultaneous detection of serum amyloid A and C-reactive protein in unprocessed blood sample. *Sensors Actuators B Chem* 2020;**320**.
36. Wang K, Wang Y, Wang C, Jia X, Li J, Xiao R, et al. Facile synthesis of high-performance SiO2@Au core–shell nanoparticles with high SERS activity. *RSC Adv* 2018;**8**:30825-31.
37. Shao B, Ma X, Zhao S, Lv Y, Hun X, Wang H, et al. Nanogapped Au(core) @ Au-Ag(shell) structures coupled with Fe3O4 magnetic nanoparticles for the detection of ochratoxin a. *Anal Chim Acta* 2018;**1033**:165-72.
38. Wang C, Li P, Wang J, Rong Z, Pang Y, Xu J, et al. Polyethylenimine-interlayered core-shell-satellite 3D magnetic microspheres as versatile SERS substrates. *Nanoscale* 2015;**7**:18694-707.
39. Wang J, Wu X, Wang C, Shao N, Dong P, Xiao R, et al. Magnetically assisted surface-enhanced Raman spectroscopy for the detection of Staphylococcus aureus based on aptamer recognition. *ACS Appl Mater Interfaces* 2015;**7**:20919-29.